JGR Planets

RESEARCH ARTICLE
10.1029/2019JE006163

Key Points:
- We construct a linearized wave model to evaluate the role of wave heating and cooling in Titan's upper atmosphere
- Wave heating by molecular diffusion is an important mechanism that influences the thermal structure of Titan's upper atmosphere
- The predicted temperature variability is likely greater than that caused by particle precipitation but still smaller than that observed

Correspondence to:
J. Cui,
cuijun7@mail.sysu.edu.cn

Citation:
Wang, X., Lian, Y., Cui, J., Richardson, M., Wu, Z., & Li, J. (2020). Temperature variability in titan's upper atmosphere: The role of wave dissipation. *Journal of Geophysical Research: Planets*, *125*, e2019JE006163. https://doi.org/10.1029/2019JE006163

Received 4 AUG 2019
Accepted 7 MAY 2020
Accepted article online 28 MAY 2020

Temperature Variability in Titan's Upper Atmosphere: The Role of Wave Dissipation

Xing Wang[1,2], Yuan Lian[3], Jun Cui[4,5], Mark Richardson[3], Zhaopeng Wu[4,5], and Jing Li[4]

[1]Key Laboratory of Lunar and Deep Space Exploration, National Astronomical Observatories, Chinese Academy of Sciences, Beijing, China, [2]School of Astronomy and Space Science, University of Chinese Academy of Sciences, Beijing, China, [3]Aeolis Research, Pasadena, CA, USA, [4]School of Atmospheric Sciences, Sun Yat-sen University, Zhuhai, China, [5]Chinese Academy of Sciences Center for Excellence in Comparative Planetology, Hefei, China

Abstract The Cassini spacecraft detected a surprisingly large temporal temperature variability of 60 Kin Titan's upper atmosphere during multiple flybys. Previous efforts examining such a variability focused on the role of radiative heating but were unable to explain the observations. Analytic estimates of the wave energy fluxes have suggested that wave heating might be an important process affecting the thermal structure of the upper atmosphere. However, approaches to date have been highly idealized and have not described wave propagation rigorously. Here, we implement an anelastic linearized wave model adopting the Wentzel-Kramers-Brillouin approximation that adequately describes wave propagation in Titan's upper atmosphere, where the observed vertical wavelengths are several times larger than the density scale height. Our results show that the wave heating and cooling rates generated by molecular diffusion of monochromatic waves are larger than those found in previous studies. The energy fluxes associated with wave dissipation can exceed that of the combined solar extreme ultraviolet (EUV) heating and HCN rotational line cooling. Compared to the wave-free, mean-state temperature, the wave energy fluxes associated with certain wave modes can produce a temperature variability as large as 20 K, which is larger than that driven by magnetospheric particle precipitation but still smaller than that observed. Our results suggest that wave heating and cooling are important processes that can modify the thermal structure of Titan's upper atmosphere and also suggest that additional processes such as wave breaking and molecular diffusion of a spectrum of waves should be considered in future studies.

Plain Language Summary The Cassini spacecraft detected a surprisingly large temperature variability of 60 Kin Titan's upper atmosphere. The roles of several notable heating and cooling mechanisms such as solar EUV radiation, charged particle precipitation, and HCN rotational line emission have been evaluated in previous works, but none of them can explain the observations. In this study, we construct a linearized wave model to evaluate the role of wave dissipation, which is well known to be able to affect the atmospheric thermal structure on various solar system objects. Previous estimates of the same mechanism have been highly idealized and have not described wave propagation adequately. Our model results show that the wave heating and cooling rates generated by molecular diffusion of monochromatic waves are substantially larger than those reported in previous studies. The wave-induced temperature variability in Titan's upper atmosphere that we obtain could reach 20 K, which is larger than that driven by charged particle precipitation from the ambient plasma, but still smaller than that observed by a factor of three. It is likely that additional wave processes such as wave breaking and molecular diffusion of a spectrum of waves make further contributions to the observed temperature variability in Titan's upper atmosphere.

1. Introduction

Titan, the largest satellite of Saturn, has a thick atmosphere that is mainly composed of N_2, CH_4, H_2, and a variety of hydrocarbons and nitriles (e.g., Niemann et al., 2005; Waite et al., 2005). Existing observations made by various instruments onboard the Cassini spacecraft and the Huygens probe revealed a complicated and highly variable thermal structure of Titan's atmosphere (e.g., Coustenis et al., 2007; Fulchignoni et al., 2005; Koskinen et al., 2011; Müller-Wodarg et al., 2008). Of particular interest for this paper is a large temperature variability of around 60 K (quoted here as the maximum difference in temperature over the observed range of 112–175 K) as implied by the Cassini Ion Neutral Mass Spectrometer (INMS) measurements made during various Titan flybys (e.g., Cui et al., 2011; Snowden et al., 2013; Westlake et al., 2011). To date, no satisfactory explanation of such a large temperature variability exists.

A number of physical processes have been considered as potential mechanisms to drive the temperature variability of about 60 K quoted above. One possible process is the heating of the upper atmosphere by solar extreme ultraviolet (EUV) radiation that is expected to cause observable solar cycle and diurnal variations (e.g., Bougher et al., 2009, 2017; Harris & Priester, 1965). However, based on the analysis of the INMS data from three individual flybys, de La Haye et al. (2007) found that the dayside temperature in Titan's upper atmosphere was lower than the nightside temperature, contradicting the hypothesis of solar EUV radiation as the dominant source of energy deposition. This was later confirmed by various analyses of a much larger INMS data set (Snowden et al., 2013; Westlake et al., 2011). Another possible process is the role of charged particle precipitation from Saturn's magnetosphere. This was initially suggested by the apparent correlation between the mean thermospheric temperature on Titan and the ambient plasma environment in terms of electron precipitation (Westlake et al., 2011). Later, Snowden and Yelle (2014) evaluated this process quantitatively and concluded that it caused a temperature variability of 7 K only in Titan's upper atmosphere. Snowden and Yelle (2014) also argued that Joule heating was insufficient to account for the observed temperature variability. The thermal structure in Titan's upper atmosphere is determined not only by heating but also by cooling, of which radiative energy loss via HCN rotational line emission is an important channel (Yelle, 1991). However, a recent investigation by Cui et al. (2016) ruled out the possibility that the INMS-derived temperature variability was connected to the variability in thermospheric HCN abundance.

It is well-known that vertically propagating waves can deposit significant momentum and energy into planetary upper atmospheres when they are damped by dissipative processes such as molecular diffusion, as exemplified in studies of the Earth (e.g., Hines, 1974; Vadas & Fritts, 2005), Mars (e.g., Fritts et al., 2006), Venus (e.g., Hinson & Jenkins, 1995), and Jupiter (e.g., French & Gierasch, 1974; Matcheva & Strobel, 1999). On Titan, typical density perturbations of 10% in the upper atmosphere were inferred from the INMS measurements of N_2 and CH_4 (Müller-Wodarg et al., 2006), likely indicative of gravity waves with characteristic wavelengths of 700 km and wave periods of 10 hr (Cui et al., 2013, 2014). Vertical wave structures have also been revealed by the Huygens Atmospheric Structure Instrument (HASI), whose data extended from the exobase down to at least 500 km above the surface (Fulchignoni et al., 2005). Müller-Wodarg et al. (2006) obtained an energy flux of 3×10^9 eV cm^{-2} s^{-1} at 1200 km, representing an upper limit to the amount of energy carried by waves. Snowden and Yelle (2014) estimated that the maximum heating rate due to viscous dissipation of waves was about 30 eV cm^{-3} s^{-1} at 1,300 km and that the maximum cooling rate due to heat flux was about 9 eV cm^{-3} s^{-1}. They suggested that these wave heating and cooling rates, though smaller than the typical solar EUV heating rate, could not be ignored.

Despite the existing efforts, a detailed calculation of energy deposition by propagating gravity waves in Titan's atmosphere is still absent. Müller-Wodarg et al. (2006) used the work done by pressure forces to estimate the wave energy flux. However, Hickey et al. (2011) showed that, for slowly traveling internal gravity waves, the wave energy fluxes were mostly dominated by the sensible heat flux. Similarly, the maximum heating rate obtained by Snowden and Yelle (2014) was based on viscous dissipation alone using the method described by Hickey et al. (2011). Nonetheless, Schubert et al. (2003) have shown that the heating rate due to viscous dissipation can be canceled by the total of wave-induced pressure gradient and wave-induced Eulerian drift for waves with small horizontal wavelengths. Furthermore, previous studies made limiting assumptions about the properties of typical waves and did not rigorously calculate the vertical distribution of the wave energy fluxes and heating/cooling rates in Titan's atmosphere. Hereby, we calculate wave perturbations using a system of linearized wave equations that are suitable for describing gravity wave motions in Titan's upper atmosphere, and estimate reversible wave energy fluxes (i.e., sensible heat flux, work done by wave-induced pressure gradient, and work done by wave-induced Eulerian drift) and irreversible wave energy flux (i.e., viscous dissipation) using the formulism of Schubert et al. (2003).

In this paper, we adopt the Wentzel-Kramers-Brillouin (WKB) approximation used by, for example, Holton and Zhu (1984) and Matcheva and Strobel (1999) to calculate the wave perturbations associated with a range of characteristic wave structures likely present in Titan's atmosphere and examine various heating/cooling sources described in Schubert et al. (2003). The WKB approximation allows us to calculate wave perturbations easily via analytic expressions instead of numerically solving ordinary differential equations. The

10.1029/2019JE006163

layout of this paper is as follows. We describe in section 2 the linearized gravity wave model and wave parameters used in this study. The model results of wave heating and cooling effects on the background atmosphere are presented in section 3, along with their relative contributions compared to radiative heating and cooling sources. Finally, we provide concluding remarks in section 4.

2. Linearized Gravity Wave Model

Internal gravity waves in the atmosphere can be dissipated by multiple mechanisms such as eddy diffusion, molecular diffusion, radiative damping, wave breaking, and dissipation induced by phase differences among various chemical species (del Genio et al., 1978; Fels, 1982; Hines, 1974; Lindzen, 1981). Wave dissipation due to molecular diffusion (including molecular viscosity and thermal conductivity) is the most important process among all these mechanisms in planetary upper atmospheres since its strength increases exponentially with altitude.

A common approach to estimate the effect of molecular diffusion is to employ a linearized wave model, which calculates wind, temperature, and pressure perturbations under the influence of molecular diffusion. The energy fluxes and heating rates derived from these perturbations can be used to evaluate the impact of various wave modes upon the background atmosphere. In Titan's upper atmosphere, the typical vertical wavelengths associated with observed wave oscillations can reach a few hundred kilometers (Müller-Wodarg et al., 2006), which are several times larger than the typical density scale height of 80 km (e.g., Cui et al., 2009). This requires a numerical model that can describe the compressibility of wave motions, for example, use of the anelastic approximation or a full-wave model. We opt to use anelastic approximation since it can filter out acoustic waves that have not been observed in Titan's atmosphere. Matcheva and Strobel (1999) adopted the linearized wave model for studying gravity waves in Jupiter's upper atmosphere. However, they only considered a Boussinesq (incompressible) fluid, where the vertical wavelength needs to be much smaller than density scale height. Therefore, in this paper, we rigorously derive the dispersion relation with the anelastic approximation following a similar procedure in Vadas and Fritts (2005) and solve for the wave perturbations using the WKB method, which is valid for slowly varying vertical wavelengths (Einaudi & Hines, 1970; Vadas & Fritts, 2005).

2.1. Model Description

Wave propagation in Titan's upper atmosphere is described by a linearized one-dimensional wave model based upon the anelastic approximation for ideal gas. We assume that the background atmosphere is plane-parallel and hydrostatically balanced. We further assume that the Coriolis effect can be ignored since Titan is a slowly rotating body and the wave periods are generally much smaller than the rotation period (Cui et al., 2014).

The atmosphere is treated as motionless due to limited information on thermospheric winds on Titan. We do recognize that winds can impact the wave propagations in many ways such as modifying wave frequency via Doppler shift, generating critical layers and affecting atmospheric stabilities. Müller-Wodarg et al. (2000, 2008) modeled the thermospheric winds using 3D global circulation model. The range of predicted wind speed (a few meters per second to 150 m s^{-1}) could be quite significant for wave propagations. The discrepancy between the vertical wavelengths measured by the Huygens probe and those derived from the INMS measurements may be an indication of the Doppler-shift effect (Müller-Wodarg et al., 2006). However, thermospheric winds on Titan are not well understood, and the presence of a wind field can greatly complicate the wave model. Therefore, we have not attempted to include background wind in this study. The resulting system of wave equations are

$$\nabla \cdot \vec{V}' - \frac{w'}{H_\rho} = 0, \tag{1}$$

$$\left[\frac{\partial}{\partial t} - \nu \nabla^2\right] u' = -\frac{1}{\rho_0}\frac{\partial p'}{\partial x}, \tag{2}$$

$$\left[\frac{\partial}{\partial t} - \nu \nabla^2\right] v' = -\frac{1}{\rho_0}\frac{\partial p'}{\partial y}, \tag{3}$$

10.1029/2019JE006163

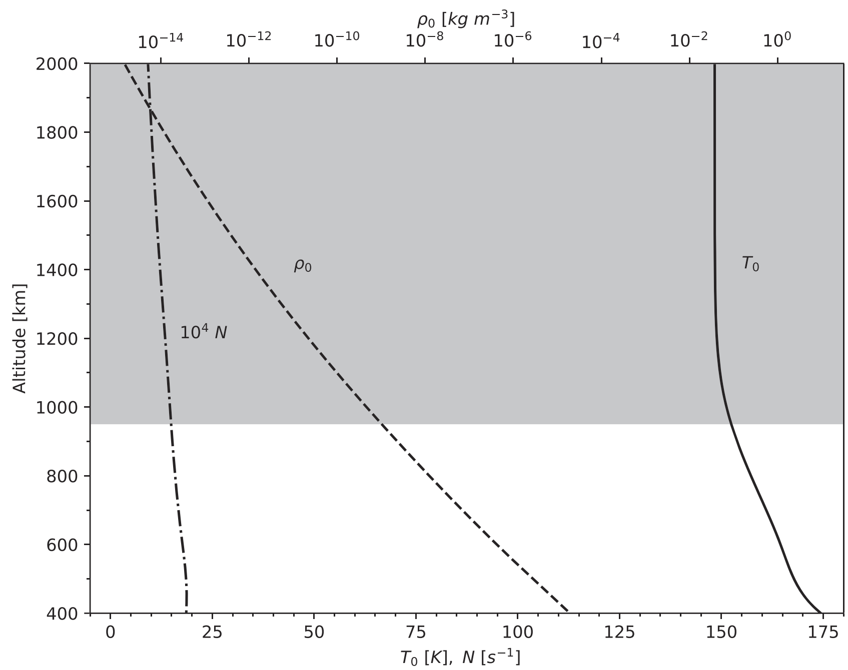

Figure 1. The vertical profiles of neutral temperature, total mass density, and Brunt-Väisälä frequency in Titan's background atmosphere over the altitude range of 400–2,000 km based on Strobel (2012). The shaded region indicates where a large temperature variability has been revealed by the INMS measurements Snowden et al. (2013).

$$\left[\frac{\partial}{\partial t} - \nu\nabla^2\right] w' = -\frac{1}{\rho_0}\frac{\partial p'}{\partial z} - \frac{\rho'}{\rho_0} g, \tag{4}$$

$$\left[\frac{\partial}{\partial t} - \frac{\nu}{Pr}\nabla^2\right] T' - \frac{1}{c_p\rho_0}\frac{\partial p'}{\partial t} = -\Gamma w', \tag{5}$$

and

$$\frac{p'}{p_0} = \frac{\rho'}{\rho_0} + \frac{T'}{T_0}, \tag{6}$$

where ρ_0, T_0, and p_0 are the reference density, temperature, and pressure of the background atmosphere adapted from Strobel (2012) including N_2, CH_4, H_2, and Ar, and ρ', T', p', and u' are the corresponding perturbations, v' and w' are the perturbations in the meridional and vertical wind velocities, $\vec{V}'$ is the perturbation in the vector wind velocity, $H_\rho = \left(-\frac{1}{\rho_0}\frac{\partial\rho_0}{\partial z}\right)^{-1}$ and $H_p = \frac{RT_0}{g}$ are the density and pressure scale heights, respectively, with g being the local gravity and R being the specific gas constant, Pr is the Prandtl number, $\Gamma = \frac{\partial T_0}{\partial z} + \frac{g}{c_p}$ is the static stability with c_p being the specific heat at constant pressure, $\nu = \mu/\rho_0$ is the kinetic viscosity with μ being the molecular dynamic viscosity. For reference, we provide in Figure 1 the vertical profiles of neutral temperature and total mass density in Titan's background atmosphere over the altitude range of 400–2,000 km. The shaded region indicates where a large temperature variability has been revealed by the INMS measurements.

Assuming wave perturbations in form of $X'(x, y, z, t) = \delta X(z) exp\left[i\left(k_x x + k_y y - \omega_0 t\right)\right]$, where X represents wave perturbations and $\delta X(z)$ is expressed as WKB solutions (e.g., Holton & Zhu, 1984) in the form of

$$\text{delta } X(z) = \Delta X(z_0)\left(\frac{k_{zr}(z_0)}{k_{zr}(z)}\right)^{\frac{1}{2}} exp\left[\int_{z_0}^{z}\left(ik_z + \frac{1}{2H_\rho}\right)dz\right], \tag{7}$$

we can obtain the dispersion relation as

$$k_z^2 = \frac{k_h^2 N^2}{\hat{\omega}(\hat{\omega} + i\beta)} - \frac{1}{4H_\rho^2} - k_h^2, \tag{8}$$

where ω_0 is the wave frequency, $k_h = \sqrt{k_x^2 + k_y^2}$ is the horizontal wavenumber with k_x and k_y being its two components, k_z is the vertical wavenumber with k_{zr} being the real part, and $N = \sqrt{\frac{g\Gamma}{T_0}}$ is the Brunt-Väisälä frequency whose altitude profile is displayed in Figure 1 for reference. $\Delta X(z_0)$ in Equation 7 is the amplitude of a prescribed perturbation (vertical velocity amplitude, ΔW, in our case) at a reference altitude, z_0, which can be iteratively determined to provide a desired maximum wave amplitude. The definitions of $\hat{\omega}$ and β follow closely those in Matcheva and Strobel (1999) with corrections accommodating the anelastic approximation, written as

$$\hat{\omega} = \omega_r + i\omega_i, \tag{9}$$

and

$$\beta = \beta_r + i\beta_i, \tag{10}$$

where

$$\omega_r = \omega_0 + 2k_{zr}\nu\left(\frac{1}{2H_\rho} - k_{zi}\right), \tag{11}$$

$$\omega_i = \nu\left[k_{zr}^2 - \left(\frac{1}{2H_\rho} - k_{zi}\right)^2 + k_h^2\right], \tag{12}$$

$$\beta_r = \left(\frac{1}{Pr} - 1\right)\omega_i, \tag{13}$$

and

$$\beta_i = 2k_{zr}\nu\left(1 - \frac{1}{Pr}\right)\left(\frac{1}{2H_\rho} - k_{zi}\right). \tag{14}$$

The meanings of the parameters in the above equations are self explanatory, which will not be detailed here. The notable difference between the dispersion relation given by Equation 8 and that in Matcheva and Strobel (1999) (see their Equation 9) is the retention of k_h in ω_i. This is retained since the vertical wavelengths can be comparable to horizontal wavelengths in Titan's upper atmosphere (Cui et al., 2013).

The dispersion relation given by Equation 8 is a sixth-order polynomial that needs to be solved numerically. It consists of three pairs of waves that describe the upward/downward propagation of buoyancy waves and waves introduced by molecular viscosity and thermal conductivity. This dispersion relation is only valid for a slowly varying background atmosphere with vertical wavelength, λ_z, comparable to or smaller than $2\pi H_\rho$ between 400 and 1,600 km in our model (Vadas & Fritts, 2005). Above 1,600 km, waves in this study are all heavily damped and the energy flux associated with wave reflection is negligible. Further calculation of the residue, d, expressed by Einaudi and Hines (1970) as

$$d = \frac{1}{2k_z^3}\frac{\partial^2 k_z}{\partial z^2} - \frac{3}{4k_z^4}\left(\frac{\partial k_z}{\partial z}\right)^2,$$

shows that it is typically several times smaller than 1 in our model, except d can be as large as 0.6 for 3-hr waves (see Table 1). This suggests that the WKB approximation is marginally applicable to Titan's upper atmosphere since the WKB approximation does not permit wave reflection but significant wave reflection is expected when $d \geq 1$ (Vadas & Fritts, 2005). Further comparison between wave energy flux and residue for all the waves shows that, from bottom up, wave energy flux decays toward zero rapidly near 1,400 km (Figure 3) where the residue reaches its peak value. This implies that wave reflection is small throughout the model domain. Therefore, the WKB solutions to the wave perturbations are not severely affected by wave reflection. Here, we adopt the WKB approximation for simplicity and defer a full-wave model that accounts for wave reflection to a future study.

Table 1
Gravity Wave Parameters and Wave Damping Altitudes

Period τ [h]	λ_h [km]	c_h [ms^{-1}]	ΔT_{max} [K]	z_{max} [km]	$\lambda_z\left(z_{max}\right)$ [km]	λ_{zm} [km]
3	600	55.6	10.0	1176	323.5	450.9
3	750	69.4	10.0	1241	468.9	522.2
3	900	83.3	10.0	1290	628.3	590.3
6	600	27.8	10.0	979	124.4	314.6
6	750	34.7	10.0	1025	161.1	345.7
6	900	41.7	10.0	1067	202.0	373.9
9	600	18.5	10.0	876	77.5	286.1
9	750	23.1	10.0	917	99.1	308.9
9	900	27.8	10.0	952	121.5	328.6

Note. Properties of the waves explored in this study. Left to right: the wave period, τ, the horizontal wavelength, λ_h, the horizontal phase speed, c_h, the maximum wave amplitude, ΔT_{max}, the altitude of maximum wave amplitude, z_{max} (hereafter denoted as the damping altitude), the vertical wavelength at the damping altitude, $\lambda_z(z_{max})$, and the mean vertical wavelength, λ_{zm}, averaged over the altitude range from 1,000 to 1,600 km. The waves are labeled for reference in the text according to their respective periods and horizontal wavelengths, denoted as 3h600km, 3h750km, 3h900km, 6h600km, 6h750km, 6h900km, 9h600km, 9h750km, and 9h900km from top to bottom.

The Equations 1 to 6 can be obtained by first solving vertical velocity perturbation w' using the WKB approximation (Equation 7). Other wave perturbations, u', T', p', and ρ', are related to w' via the following polarization relations under anelastic approximation

$$u' = -\frac{ik_x}{k_h^2}\left(-ik_z + \frac{1}{2H_\rho}\right)w', \tag{15}$$

$$T' = -\frac{i}{\hat{\omega} + i\beta}\left[\Gamma + \frac{\omega_0\hat{\omega}}{c_p k_h^2}\left(-ik_z + \frac{1}{2H_p}\right)\right]w', \tag{16}$$

$$p' = -\frac{i\rho_0\hat{\omega}}{k_h^2}\left(-ik_z + \frac{1}{2H_\rho}\right)w', \tag{17}$$

and

$$\frac{\rho'}{\rho_0 = i\left\{\frac{\Gamma}{T_0(\hat{\omega}+i\beta)} - \frac{\hat{\omega}}{k_h^2}\left[\frac{1}{RT_0} - \frac{\omega_0}{T_0 c_p(\hat{\omega}+i\beta)}\right]\left(-ik_z + \frac{1}{2H_p}\right)\right\}w'}. \tag{18}$$

We only consider monochromatic waves in our model. This means that we consider one wave at a time and these waves do not coexist. Each wave is defined by a horizontal wavelength, λ_x, a wave period, τ (equivalently, a wave frequency, $\omega_0 = \frac{2\pi}{\tau}$), and a prescribed maximum amplitude, which can be used to solve the dispersion relation (Equation 8) and wave perturbations (Equations 15 to 18). Finally, we derive the energy fluxes and heating/cooling rates associated with these wave perturbations as an intuitive way to demonstrate the effect of wave dissipation on the thermal structure of Titan's upper atmosphere.

2.2. Model Parameters

The range of gravity wave modes considered in this paper is guided by the earlier work of Cui et al. (2014), who showed that the gravity wave periods in the upper atmosphere ranged from about 1.5 to 10 Earth hours. These wave periods are substantially smaller than those associated with diurnal tides, as studied by Müller-Wodarg et al. (2006). We restrict the calculations to these periods for a couple of reasons. First, there is a substantial uncertainty as to the dominant modes of planetary-scale waves, for instance, associated with

10.1029/2019JE006163

stratospheric superrotation (e.g., Newman et al., 2011). Second, the low-frequency and long-wavelength nature of planetary-scale waves invalidates the beta-plane and plane-parallel approximations in our model.

In this study, we specifically examine nine wave modes (Table 1). These waves are selected to produce a reasonable range of vertical wavelengths comparable to those retrieved from the observations. For simplicity, the wave amplitude, ΔT, is fixed as 10 K, which is an upper limit of the average amplitude derived from the INMS N_2 and CH_4 density measurements (Müller-Wodarg et al., 2006). This wave amplitude is also comparable to the amplitude of density perturbations used by Snowden and Yelle (2014), as a density perturbation of 10% is roughly equivalent to a temperature perturbation of 15 K for an incompressible atmosphere. The physical properties of the background atmosphere are assumed to be constant, except where stated. Similar to Müller-Wodarg et al. (2006) and Snowden and Yelle (2014), we choose a specific gas constant of $R =$ 290 J $(\text{kg K})^{-1}$, a specific heat at constant pressure of $c_p = 1{,}450$ J $(\text{kg K})^{-1}$, a molecular viscosity of $\mu =$ 110^{-5} kg $(\text{m s})^{-1}$ typical for an N_2 atmosphere at 149 K, and a Prandtl number of $P_r = 0.69$. Unlike previous works, we take into account the vertical variation of acceleration due to gravity, $g = GM/(z + R_T)^2$, which primarily affects the density scale height and the Brunt-Väisälä frequency. Here G is the gravitational constant, z is the altitude, M and R_T are the mass and solid body radius of Titan, respectively.

2.3. Wave Heating/Cooling of the Background Atmosphere

In an atmosphere absent of any wave damping mechanisms, the energy and momentum fluxes carried by vertically propagating waves remain unchanged from those injected in the wave source region. The presence of molecular diffusion suppresses the growth of wave amplitudes and therefore reduces the magnitude of energy and momentum fluxes along the direction of wave propagation. In addition to the decaying trend due to damping, phase differences between wave perturbations creates convergence and divergence patterns of wave energy and momentum fluxes, which lead to the heating and cooling of the background atmosphere. However, the vertically integrated heating and cooling rates do not result in net heating and cooling of the background atmosphere due to the conservation of energy.

We calculate the total wave heating and cooling rates following the formulism of Hickey et al. (2000) and Schubert et al. (2003), written as

$$H_{tot} \equiv -\frac{\partial F_{tot}}{\partial z} = -\frac{\partial}{\partial z}\left(F_h + F_v + F_p + F_d\right). \tag{19}$$

In Equation 19, $F_h = \rho_0 c_p \langle w'T' \rangle$ is the sensible heat flux, $F_v + -\int_z^\infty \langle \sigma' : \nabla \vec{V}' \rangle dz$ is the energy flux associated with viscous dissipation where σ' is the molecular viscous stress tensor (see Lian & Yelle, 2019 for detailed expression of σ'), $F_p = -\int_z^\infty \langle \vec{V}' \cdot \nabla p' \rangle dz$ is the work done per unit time by wave-induced pressure gradients, and $F_d = -\int_z^\infty \langle w' \rho' \rangle g dz$ is the work done per unit time by wave-induced Eulerian drift. The angled bracket $\langle\rangle$ means $\langle AB \rangle = \frac{1}{2} Re(AB^*)$, where A and B are arbitrary complex functions and * denotes the complex conjugate.

3. Results

We examine the effect of molecular diffusion on vertically propagating gravity waves and its contribution to the background atmosphere in three ways. First, we identify waves that have damping altitudes ranging from 1,000 to 1,500 km, where a large temperature variability was revealed by the INMS measurements made during Cassini flybys with Titan (e.g., Snowden et al., 2013; Westlake et al., 2011), and that have vertical wavelengths ranging from 170 to 360 km at those damping altitudes, also motivated by the INMS measurements (e.g., Müller-Wodarg et al., 2006). Second, we compare the wave heating and cooling rates to that required to maintain the vertical gradient of the globally averaged temperature. The temperature variability due to the wave energy fluxes are also calculated. Third, we compare the wave heating and cooling rates to the EUV heating rates estimated from the INMS densities of various chemical constituents in Titan's upper atmosphere (e.g., Cui et al., 2009), and derive the temperature profiles using all three major heating and cooling sources between 1,000 and 1,400 km, that is, EUV heating, HCN cooling, and gravity wave heating and cooling.

3.1. Wave Damping Properties

Figure 2 shows the wave amplitudes as a function of altitude for the nine waves explored in this study. The corresponding vertical wavelengths, $\lambda_z\left(z_{max}\right)$, at the wave damping altitudes, z_{max}, are provided in Table 1.

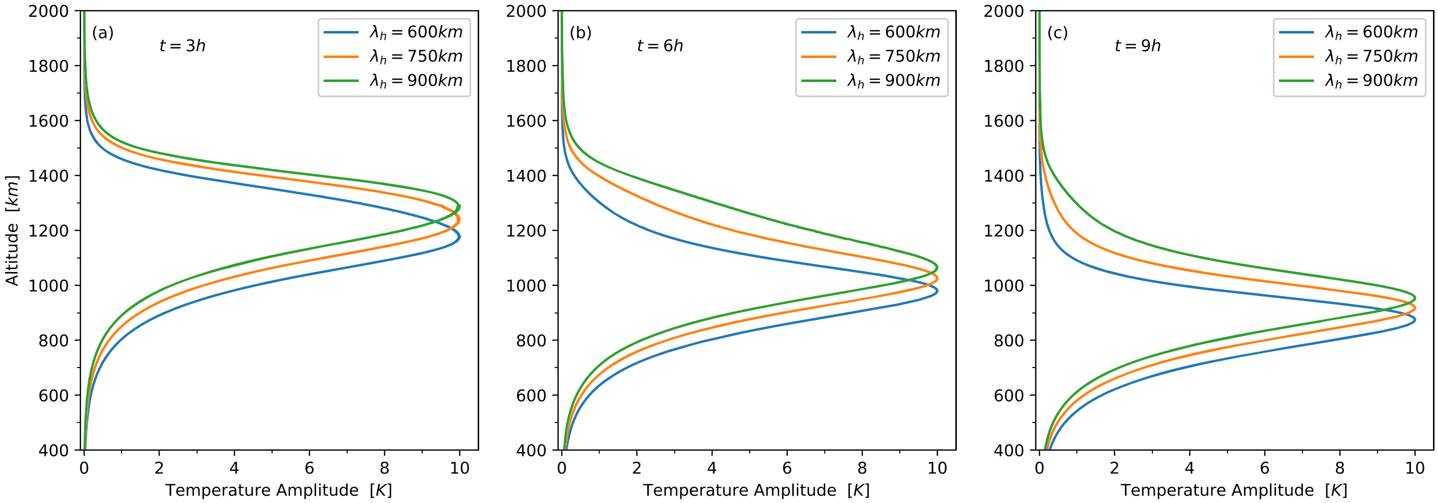

Figure 2. Amplitude of the wave temperature perturbation as a function of altitude: (a) 3-hr waves; (b) 6-hr waves; (c) 9-hr waves. The location of the maximum wave amplitude is the damping altitude where the growth of the wave perturbation is effectively suppressed by molecular diffusion.

We use the naming convention *x*h*y*km to simplify the description of each wave, where *x*h is the prescribed wave period in *x* hours and *y*km is the prescribed horizontal wavelength in *y* kilometers (also see captions in Table 1). A general trend is that gravity waves with faster horizontal phase speeds (equivalently longer vertical wavelengths) can propagate to higher altitudes before they are damped by molecular diffusion. This trend is consistent with previous studies such as Vadas and Fritts (2005) and Lian and Yelle (2019). The damping altitudes of these waves range from 900 to about 1,300 km, above which the wave amplitudes stop growing.

Similar to previous studies (e.g., Hickey et al., 2000), the vertical wavelengths of these upward propagating waves remain nearly unchanged until the waves reach their damping altitudes, above which the vertical wavelengths are stretched to larger values due to stronger molecular diffusion (not shown). We average vertical wavelengths, λ_z, between 1,000 and 1,600 km in order to compare the modeled waves to those observed (Table 1). The majority of the mean vertical wavelengths, λ_{zm}, are comparable to the observed range of 170–360 km (Müller-Wodarg et al., 2006) except those of the 3-hr waves with phase speeds greater than 50 m s^{-1}. However, we have retained the 3h600km wave since the vertical wavelength, $\lambda_z = 323.5$ km, at its damping altitude, $z_{max} = 1{,}176$ km, also satisfies the observed range. The nominal wave modes used throughout the rest of this paper are thus the 3h600km wave, and all of the 6- and 9-hr waves. It should be noted that a wider range of gravity wave modes could meet the requirement of the observed vertical wavelengths. Furthermore, the modeled wave properties can be affected by the choice of the background atmosphere and the inclusion of extra physical processes such as radiative damping. Here we choose a limited number of waves for reasons of practicality and in order to illustrate the importance of wave damping by molecular diffusion as a standalone process.

3.2. Wave Heating and Cooling

The general relationship between the wave damping altitude and the energy flux (heating rate) is such that waves with lower damping altitudes require larger upward energy fluxes in order to produce the fixed 10 K wave amplitude. These waves also induce larger downward energy fluxes. The convergence and divergence of the wave energy fluxes produce larger heating and cooling rates accordingly.

Figure 3 shows the energy fluxes and heating rates associated with the damping of waves 3h600km, 6h600km, and 9h600km as examples. For all the three waves, the energy fluxes due to the work done by wave-induced pressure perturbation, F_p, and the work done by wave-induced Eulerian drift, F_d, nearly cancel at all altitudes despite being individually large (Figures 3a, 3b, and 3c). F_p and F_d are reversible mechanical energy fluxes that should have perfect cancelation in an atmosphere without any dissipation (Schubert et al., 2003). However, the cooling effect of F_p exceeds the heating effect of F_d when dissipation is present (Lian & Yelle, 2019; Schubert et al., 2003).

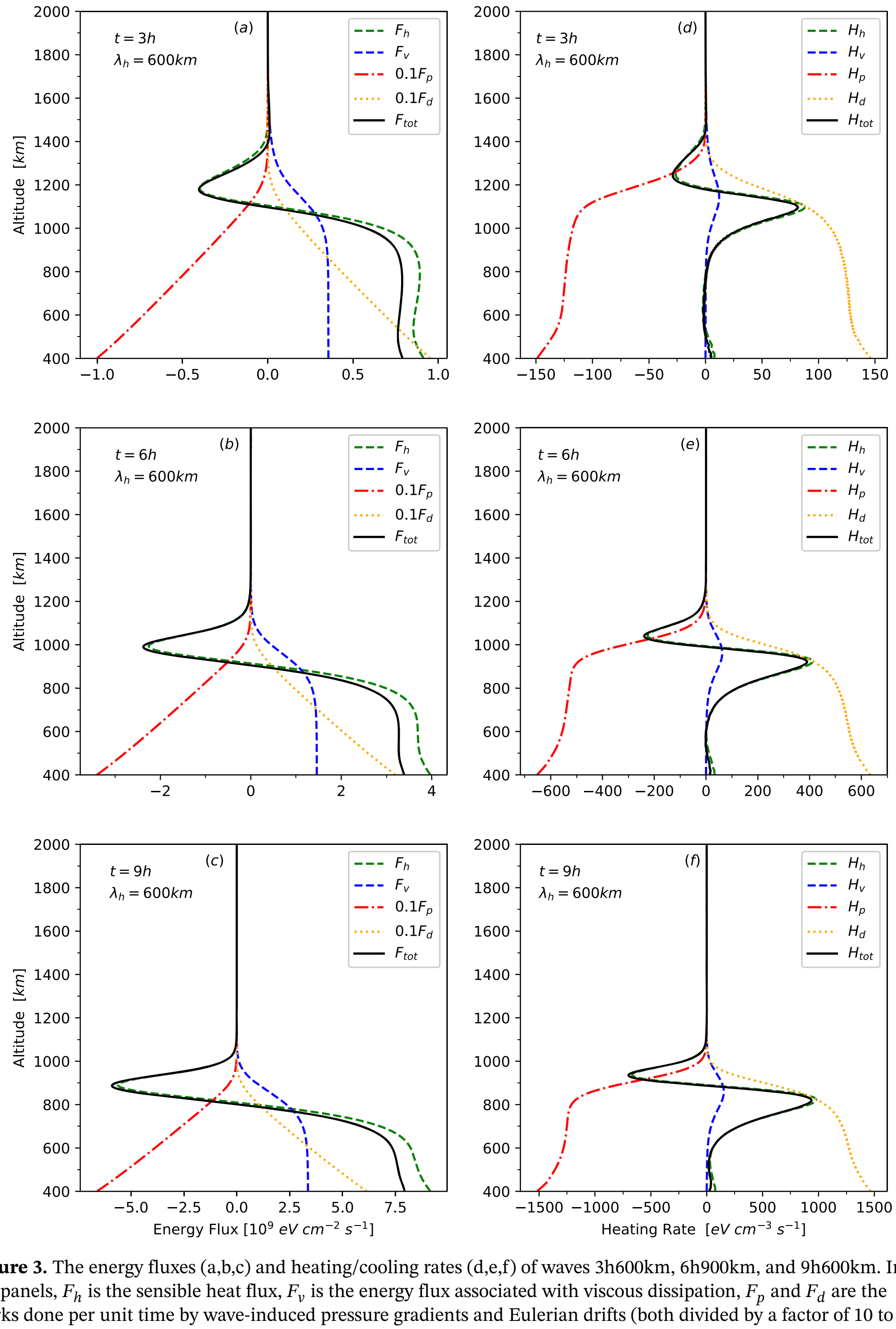

Figure 3. The energy fluxes (a,b,c) and heating/cooling rates (d,e,f) of waves 3h600km, 6h900km, and 9h600km. In the left panels, F_h is the sensible heat flux, F_v is the energy flux associated with viscous dissipation, F_p and F_d are the works done per unit time by wave-induced pressure gradients and Eulerian drifts (both divided by a factor of 10 to improve visibility), and F_{tot} is the total energy flux. H_h, H_v, H_p, H_d, and H_{tot} in the right panels are the respective heating/cooling rates.

The small residual of these two fluxes F_p and F_d along with viscous dissipation, F_v, results in a total energy flux, F_{tot}, that is slightly smaller than the sensible heat flux, F_h. The total upward energy flux at the bottom of the model domain (400 km) is about 0.8×10^9 eV cm^{-2} s^{-1}, 3.3×10^9 eV cm^{-2} s^{-1}, and 8×10^9 eV cm^{-2} s^{-1} for waves 3h600km, 6h600km, and 9h600km, respectively. This increase in upward energy flux is due to the decreasing damping altitudes of these waves (Table 1), where waves with a lower damping altitude require a larger energy input to produce the same $10\,K$ amplitude in a denser atmosphere.

The maximum wave energy fluxes carried by the 6- and 9-hr waves in our model are larger than the value of 1.2×10^9 eV cm^{-2} s^{-1} estimated by Müller-Wodarg et al. (2006) due to differences in the model approximations and wave parameters. For instance, Müller-Wodarg et al. (2006) considered a planetary-scale wave with a horizontal wavelength of 12,000 km (derived from their equation, $\lambda_h = 2\pi\,(R_T + z)/s$, where $s = 2$) and a period of about one Titan hour, and they used the formulism of Matcheva and Strobel (1999) for the work done by pressure forces to estimate the amount of energy carried by this wave. While the selection of this wave can be supported by numerical model results (Newman et al., 2011), the Matcheva and Strobel (1999) formulism requires the Boussinesq approximation to be valid as evident from their expression for the thermodynamic equation and the equation of state. That is, the vertical wavelength has to be much smaller than the density scale height to ensure that the wave motions can be treated as incompressible, a condition that is not satisfied within Titan's upper atmosphere according to existing observations. Recognizing these differences, we recalculate the properties of wave propagation using our anelastic wave model and the same wave parameters used by Müller-Wodarg et al. (2006). Assuming the atmosphere is motionless and waves have a deep origin (e.g., waves originate from the stratosphere), we find that these planetary-scale waves experience significant damping before they reach thermospheric altitudes, characterized by wave damping altitudes of around 500 km, and that the wave heating and cooling effects vanish within the mesosphere.

The wave energy fluxes in our model, while smaller than the solar EUV fluxes (e.g., Snowden & Yelle, 2014), are more significant in terms of their heating and cooling effects on the mean-state atmosphere than previously thought. Figures 3d, 3e, and 3f show the heating and cooling rates derived from the convergence and divergence of the energy fluxes. Wave 3h600km produces a maximum total heating rate of 80 eV cm^{-3} s^{-1} near 1,100 km and a maximum cooling rate of 30 eV cm^{-3} s^{-1} near 1,250 km. Wave 6h600km produces a maximum total heating rate of 400 eV cm^{-3} s^{-1} near 900 km and a maximum cooling rate of 200 eV cm^{-3} s^{-1} near 1,100 km. Wave 9h900km produces a maximum total heating rate of 1,000 eV cm^{-3} s^{-1} near 800 km and a maximum cooling rate of 750 eV cm^{-3} s^{-1} near 950 km. All of the waves generate heating and cooling rates much larger than the maximum heating rate of 30 eV cm^{-3} s^{-1} and the maximum cooling rate of 9 eV cm^{-3} s^{-1} estimated by Snowden and Yelle (2014). In fact, the values in Snowden and Yelle (2014) would be lower if our wave parameters were used instead. For instance, the vertical wavelength ($\lambda_z(z_{max}) =$ 323 km) and the relative wave amplitude (~6.7%) of wave 3h600km leads to a maximum cooling rate of 4.3 eV cm^{-3} s^{-1} using Snowden and Yelle's (2014) method. The difference between our work and theirs might be connected to the way that the wave energy fluxes were estimated. Compared to our model, Snowden and Yelle (2014) used a simplified equation from Hickey et al. (2011) as a crude approximation to wave heating by sensible heat flux only and ignored wave propagation in an atmosphere with vertically variable physical quantities such as density and temperature.

3.3. Effect of Wave Heating/Cooling on the Thermal Structure

A quick comparison between the wave heating/cooling rates in our model and the solar EUV heating rates reported in previous studies (e.g., Strobel, 2008; Snowden & Yelle, 2014) suggests that the heating and cooling effects of certain waves could become dominant in Titan's upper atmosphere. Taking wave 3h600km as an example, the wave heating rate peaks at 1,100 km with a magnitude of 80 eV cm^{-3} s^{-1} and the wave cooling rate peaks at 1240 km with a magnitude of 30 eV cm^{-3} s^{-1} (see Figure 2d), whereas the solar EUV heating rates are 65 eV cm^{-3} s^{-1} and 20 eV cm^{-3} s^{-1} at these two altitudes according to Snowden and Yelle (2014) (see their Figure 7a).

In order to examine more rigorously the impact of wave heating/cooling on the temperature variability of Titan's upper atmosphere as implied by the INMS data, we use the energy balance equation to derive the

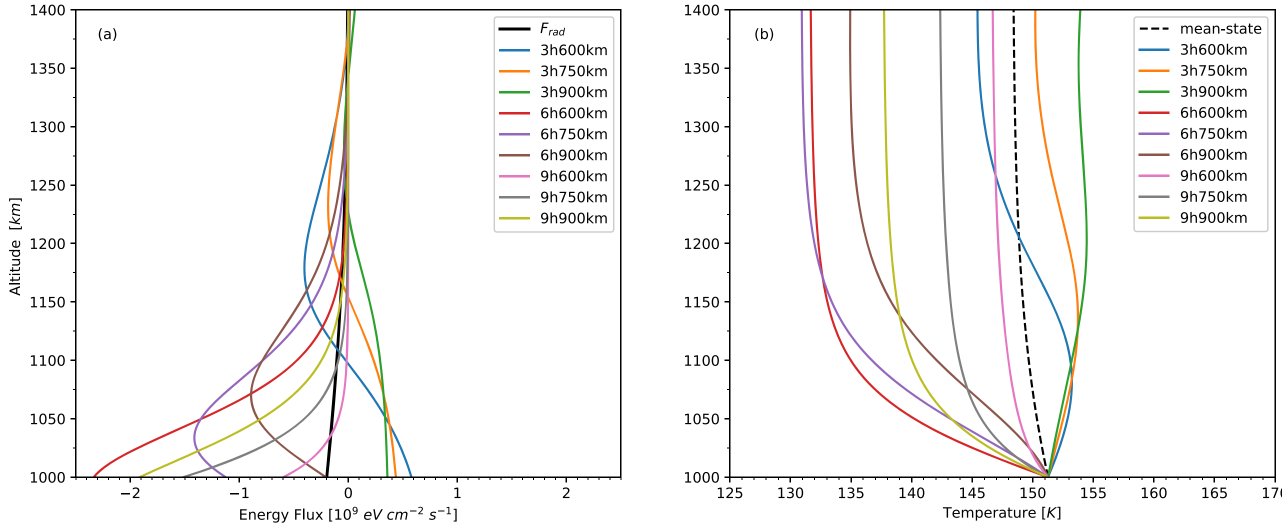

Figure 4. Energy fluxes and the mean-state temperatures associated with these energy fluxes. (a) Wave energy fluxes associated with various wave modes, as well as the net radiative energy flux contributed by both solar EUV heating and HCN cooling; (b) Mean-state temperature profiles integrated from the total energy fluxes.

wave-induced temperature profile above 1,000 km. Such an equation assumes the sum of all energy fluxes, including the wave energy flux, the radiative energy flux, and the conductive heat flux, to be zero, written as

$$F_w^i + F_{rad} = k_m \frac{\partial T_m^i}{\partial z}, \tag{20}$$

where i denotes a wave mode, T_m^i is the mean-state temperature, F_w^i is the wave energy flux, F_{rad} is the net radiative energy flux contributed by both EUV heating and HCN cooling, and k_m is the thermal conductivity parameterized as $k_m = 27.21 \times 10^{-5} T_0^{0.8}\,\mathrm{J\,(m\,K\,s)^{-1}}$ (Müller-Wodarg et al., 2006; Snowden et al., 2013). It should be noted that the calculation of F_{rad} may be affected by the choice of the mean-state temperature T_m^i. In this case, solving Equation 20 becomes complicated unless a simple analytical relation between F_{rad} and T_m^i can be provided. For simplicity, we assume F_{rad} is independent of wave motions, and it is calculated from the reference temperature used in the linearized wave model. Since the reference temperature is near isothermal over the altitude range of interest (Strobel, 2012), close balance between solar EUV heating and HCN rotational line cooling is expected (Yelle, 1991).

The net radiative energy flux obtained in such a manner is displayed in Figure 3a, superimposed on the wave energy fluxes of all the nine wave modes considered in this study. The figure demonstrates clearly the role of wave heating and cooling on the energy balance of Titan's upper atmosphere. We ought to emphasize that both solar EUV heating and HCN cooling likely exceed the effect of wave dissipation if they were considered as standalone processes, but wave dissipation still has a profound influence on the thermal structure due to the cancelation of the two radiative heating/cooling sources.

The wave-induced, mean-state temperature profiles derived from the energy fluxes associated with various wave modes exhibit a considerable variability of 20 K between 1,000 and 1,400 km, using the net radiative energy flux derived above and assumed to be independent of the presence of waves. These profiles are presented in Figure 4b, along with the wave-free, mean-state profile. Among the nominal wave modes, wave 6h750km produces the largest temperature difference (about 20 K) relative to the reference temperature of 150 K at 1,400 km. This 20 K difference is comparable to the 19 K difference resulting from magnetospheric particle precipitation (Westlake et al., 2011) and is about three times larger than the 7 K difference estimated by Snowden and Yelle (2014) for the temperature variability driven by the same mechanism. A larger temperature variability can be found if we consider the two waves with vertical wavelengths greater than the observed upper limit (~360 km), that is, the maximum temperature difference between wave 6h750km and wave 3h900km is about 23 K. Nonetheless, the temperature difference produced by wave dissipation in our study is still smaller than the observed variability of 60 K (e.g., Snowden et al., 2013; Westlake et al., 2011).

4. Conclusion and Discussion

Existing Cassini INMS measurements suggest a temperature variability as large as 60 Kin Titan's upper atmosphere, of which the driving source is still unknown (e.g., Cui et al., 2011; de La Haye et al., 2007; Müller-Wodarg et al., 2008; Snowden et al., 2013; Westlake et al., 2011). This fact, along with the extensive observations of strong wave structures in Titan's atmosphere (e.g., Cui et al., 2013, 2014; Fulchignoni et al., 2005; Koskinen et al., 2011; Müller-Wodarg et al., 2006), motivates us to examine the effect of these waves on the atmospheric energy balance from 1,000 km up to the exobase. In this study, we use a linearized wave model to estimate the heating and cooling of the mean-state atmosphere by molecular diffusion of vertically propagating gravity waves. We find that wave dissipation is an important source of energy that modifies the local thermal structure. Using previous INMS-based analyses of density and temperature perturbations as a constraint (Cui et al., 2014; Müller-Wodarg et al., 2006), we select nine typical wave modes to calculate the strength of wave heating and cooling. The maximum heating and cooling rates associated with molecular diffusion of some of the examined waves are much larger than those estimated in previous studies (Müller-Wodarg et al., 2006; Snowden & Yelle, 2014). Despite that the wave energy fluxes could be smaller than the EUV energy flux overall at certain altitudes and for certain wave modes, they become significant compared to net radiative heating when the effect of HCN cooling is also taken into account.

The maximum difference between the wave-induced, mean-state temperature and the wave-free, mean-state temperature is about 20 K, which is much larger than that associated with variable magnetospheric particle precipitation (Snowden & Yelle, 2014). However, the difference is still smaller than the INMS-derived temperature variability of 60 K. This motivates us to include other important wave processes in our model. One of the potential processes is wave breaking. Similar to the effect of molecular diffusion on gravity waves, wave breaking due to wave saturation or existence of critical layers can cause both heating and cooling of the atmosphere (e.g., Schoeberl et al., 1983). In Titan's upper atmosphere, most waves do not appear to be saturated but occasionally some waves come very close to saturation, for example, the gradient of temperature perturbation measured during the Cassini T5 flyby was very close to the dry adiabatic lapse rate at about 1,100 km (Müller-Wodarg et al., 2006). It is not known whether this type of wave oscillation is a result of the combined effect of molecular diffusion and wave saturation. Another possible process is multiwave dissipation. In this study, we only consider monochromatic waves. In reality, waves often propagate as a packet that contains multiple wave modes. The superposition of energy fluxes associated with multiple wave modes can potentially produce a large temperature variability (Lian & Yelle, 2019). These processes are beyond the scope of the present study, but will be considered in a future work.

So far we have focused upon the effect of wave heating and cooling of the mean-state atmosphere, but ignored the sources of these waves. Based on our calculations, planetary-scale waves generated by either Saturn's gravitational tide (Tokano & Neubauer, 2002) or barotropic instabilities (Newman et al., 2011) are damped by molecular diffusion significantly before they reach 700 km. However, we cannot rule out the contribution of these waves to thermospheric heating/cooling since the presence of background wind field, when properly configured, could lead to higher wave damping altitude when wave phase speed relative to the background atmosphere becomes larger due to Doppler-shift effect. Therefore, the propagation of these waves shall be revisited with a prescribed background wind field predicted by numerical models, for example, Müller-Wodarg et al. (2008). The interaction between near surface wind and terrain variation may generate orographic waves with horizontal wavelengths comparable to those in our model. These waves are stationary relative to the ground but their propagation is characterized by the intrinsic wave frequency (Doppler-shift wave frequency) as long as the background wind speed is nonzero. For instance, assuming that the orographically generated wave has a horizontal wavelength of 600 km, then the intrinsic wave period is about 8 hr for a background wind speed of 20 $m\ s^{-1}$. These wave periods and horizontal wavelengths are comparable to those examined in this study. Moreover, transient waves with horizontal scales and periods similar to the wave modes in our study may also be generated by atmospheric instabilities such as shear instabilities. Clearly, detailed terrain feature analysis with the assistance of global circulation modeling and numerical models that can resolve wavelength of a few hundred kilometers are required to understand the generation of orographic waves and transient waves in Titan's atmosphere.

Data Availability Statement

The Cassini data used in this study are available at the Planetary Plasma Interactions (PPI) node of the NASA Planetary Data System (PDS) public archives (https://pds-ppi.igpp.ucla.edu). The Python code used to calculate the wave heating and cooling rates can be accessed via Cui, Jun; Wu, Xiaoshu (2020), Wave heating and cooling in Titan's upper atmosphere, Mendeley Data, V1 (doi: 10.17632/72wnfxmm26.1).

Acknowledgments

This work is supported by the B-type Strategic Priority Program No. XDB41000000 funded by the Chinese Academy of Sciences and the pre-research project on Civil Aerospace Technologies No. D020105 funded by China's National Space Administration. J.C. also acknowledges supports from the National Science Foundation of China through grants 41525015 and 41774186.

References

Bougher, S. W., McDunn, T. M., Zoldak, K. A., & Forbes, J. M. (2009). Solar cycle variability of Mars dayside exospheric temperatures: Model evaluation of underlying thermal balances. *Geophysical Research Letters*, *36*, L05201. https://doi.org/10.1029/2008GL036376

Bougher, S. W., Roeten, K. J., Olsen, K., Mahaffy, P. R., Benna, M., Elrod, M., et al. (2017). The structure and variability of Mars dayside thermosphere from MAVEN NGIMS and IUVS measurements: Seasonal and solar activity trends in scale heights and temperatures. *Journal of Geophysical Research: Space Physics*, *122*, 1296–1313. https://doi.org/10.1002/2016JA023454

Coustenis, A., Achterberg, R. K., Conrath, B. J., Jennings, D. E., Marten, A., Gautier, D., et al. (2007). The composition of Titan's stratosphere from Cassini/CIRS mid-infrared spectra. *Icarus*, *189*, 35–62. https://doi.org/10.1016/j.icarus.2006.12.022

Cui, J., Cao, Y. T., Lavvas, P. P., & Koskinen, T. T. (2016). The variability of HCN in Titan's upper atmosphere as implied by the Cassini Ion-Neutral Mass Spectrometer measurements. *The Astrophysical Journal Letters*, *826*, L5. https://doi.org/10.3847/2041-8205/826/1/L5

Cui, J., Lian, Y., & Müller-Wodarg, I. C. F. (2013). Compositional effects in Titan's thermospheric gravity waves. *Geophysical Research Letters*, *40*, 43–47. https://doi.org/10.1029/2012GL054621

Cui, J., Yelle, R. V., Li, T., Snowden, D. S., & Müller-Wodarg, I. C. F. (2014). Density waves in Titan's upper atmosphere. *Journal of Geophysical Research: Space Physics*, *119*, 490–518. https://doi.org/10.1002/2013JA019113

Cui, J., Yelle, R. V., Müller-Wodarg, I. C. F., Lavvas, P. P., & Galand, M. (2011). The implications of the H_2 variability in Titan's exosphere. *Journal of Geophysical Research*, *116*, A11324. https://doi.org/10.1029/2011JA016808

Cui, J., Yelle, R. V., Vuitton, V., Waite, J. H., Kasprzak, W. T., Gell, D. A., et al. (2009). Analysis of Titan's neutral upper atmosphere from Cassini Ion Neutral Mass Spectrometer measurements. *Icarus*, *200*, 581–615. https://doi.org/10.1016/j.icarus.2008.12.005

de La Haye, V., Waite, J. H., Johnson, R. E., Yelle, R. V., Cravens, T. E., Luhmann, J. G., et al. (2007). Cassini Ion and Neutral Mass Spectrometer data in Titan's upper atmosphere and exosphere: Observation of a suprathermal corona. *Journal of Geophysical Research*, *112*, A07309. https://doi.org/10.1029/2006JA012222

del Genio, A. D., Straus, J. M., & Schubert, G. (1978). Effects of wave-induced diffusion on thermospheric acoustic-gravity waves. *Geophysical Research Letters*, *5*, 265–267. https://doi.org/10.1029/GL005i004p00265

Einaudi, F., & Hines, C. O. (1970). WKB approximation in application to acoustic gravity waves. *Canadian Journal of Physics*, *48*, 1458–1471. https://doi.org/10.1139/p70-185

Fels, S. B. (1982). A parameterization of scale-dependent radiative damping rates in the middle atmosphere. *Journal of Atmospheric Sciences*, *39*, 1141–1152. https://doi.org/10.1175/1520-0469(1982)039<1141:APOSDR>5872.0.CO;2

French, R. G., & Gierasch, P. J. (1974). Waves in the Jovian upper atmosphere. *Journal of Atmospheric Sciences*, *31*, 1707–1712. https://doi.org/10.1175/1520-0469(1974)031<1707:WITJUA>5902.0.CO;2

Fritts, D. C., Wang, L., & Tolson, R. H. (2006). Mean and gravity wave structures and variability in the Mars upper atmosphere inferred from Mars Global Surveyor and Mars Odyssey aerobraking densities. *Journal of Geophysical Research*, *111*, A12304. https://doi.org/10.1029/2006JA011897

Fulchignoni, M., Ferri, F., Angrilli, F., Ball, A. J., Bar-Nun, A., Barucci, M. A., et al. (2005). In situ measurements of the physical characteristics of Titan's environment. *Nature*, *438*, 785–791. https://doi.org/10.1038/nature04314

Harris, I., & Priester, W. (1965). Of the diurnal variation of the upper atmosphere. *Journal of Atmospheric Sciences*, *22*, 3–10. https://doi.org/10.1175/1520-0469(1965)022<0003:OTDVOT>6012.0.CO;2

Hickey, M. P., Walterscheid, R. L., & Schubert, G. (2000). Gravity wave heating and cooling in Jupiter's thermosphere. *Icarus*, *148*, 266–281. https://doi.org/10.1006/icar.2000.6472

Hickey, M. P., Walterscheid, R. L., & Schubert, G. (2011). Gravity wave heating and cooling of the thermosphere: Sensible heat flux and viscous flux of kinetic energy. *Journal of Geophysical Research*, *116*, A12326. https://doi.org/10.1029/2011JA016792

Hines, C. O. (1974). *The upper atmosphere in motion*.

Hinson, D. P., & Jenkins, J. M. (1995). Magellan radio occultation measurements of atmospheric waves on Venus. *Icarus*, *114*, 310–327. https://doi.org/10.1006/icar.1995.1064

Holton, J. R., & Zhu, X. (1984). A further study of gravity wave induced drag and diffusion in the mesosphere. *Journal of Atmospheric Sciences*, *41*, 2653–2662. https://doi.org/10.1175/1520-0469(1984)041<2653:AFSOGW>2.0.CO;2

Koskinen, T. T., Yelle, R. V., Snowden, D. S., Lavvas, P., Sandel, B. R., Capalbo, F. J., et al. (2011). The mesosphere and lower thermosphere of Titan revealed by Cassini/UVIS stellar occultations. *Icarus*, *216*, 507–534. https://doi.org/10.1016/j.icarus.2011.09.022

Lian, Y., & Yelle, R. V. (2019). Damping of gravity waves by kinetic processes in Jupiter's thermosphere. *Icarus*, *329*, 222–245. https://doi.org/10.1016/j.icarus.2019.04.001

Lindzen, R. S. (1981). Turbulence and stress owing to gravity wave and tidal breakdown. *Journal of Geophysical Research*, *86*, 9707–9714. https://doi.org/10.1029/JC086iC10p09707

Matcheva, K. I., & Strobel, D. F. (1999). Heating of Jupiter's thermosphere by dissipation of gravity waves due to molecular viscosity and heat conduction. *Icarus*, *140*, 328–340. https://doi.org/10.1006/icar.1999.6151

Müller-Wodarg, I. C. F., Yelle, R. V., Borggren, N., & Waite, J. H. (2006). Waves and horizontal structures in Titan's thermosphere. *Journal of Geophysical Research*, *111*, A12315. https://doi.org/10.1029/2006JA011961

Müller-Wodarg, I. C. F., Yelle, R. V., Cui, J., & Waite, J. H. (2008). Horizontal structures and dynamics of Titan's thermosphere. *Journal of Geophysical Research*, *113*, E10005. https://doi.org/10.1029/2007JE003033

Müller-Wodarg, I. C. F., Yelle, R. V., Mendillo, M., Young, L. A., & Aylward, A. D. (2000). The thermosphere of Titan simulated by a global three-dimensional time-dependent model. *Journal of Geophysical Research*, *105*(A9), 20“833–20,856. https://doi.org/10.1029/2000JA000053

Newman, C. E., Lee, C., Lian, Y., Richardson, M. I., & Toigo, A. D. (2011). Stratospheric superrotation in the TitanWRF model. *Icarus*, *213*, 636–654. https://doi.org/10.1016/j.icarus.2011.03.025

Niemann, H. B., Atreya, S. K., Bauer, S. J., Carignan, G. R., Demick, J. E., Frost, R. L., et al. (2005). The abundances of constituents of Titan's atmosphere from the GCMS instrument on the Huygens probe. *Nature*, *438*(7069), 779–784. https://doi.org/10.1038/nature04122

Schoeberl, M. R., Strobel, D. F., & Apruzese, J. P. (1983). A numerical model of gravity wave breaking and stress in the mesosphere. *Journal of Geophysical Research*, *88*, 5249–5259. https://doi.org/10.1029/JC088iC09p05249

Schubert, G., Hickey, M. P., & Walterscheid, R. L. (2003). Heating of Jupiter's thermosphere by the dissipation of upward propagating acoustic waves. *Icarus*, *163*, 398–413. https://doi.org/10.1016/S0019-1035(03)00078-2

Snowden, D., & Yelle, R. V. (2014). The thermal structure of Titan's upper atmosphere, II: Energetics. *Icarus*, *228*, 64–77. https://doi.org/10.1016/j.icarus.2013.08.027

Snowden, D., Yelle, R. V., Cui, J., Wahlund, J.-E., Edberg, N. J. T., & Ågren, K. (2013). The thermal structure of Titan's upper atmosphere, I: Temperature profiles from Cassini INMS observations. *Icarus*, *226*, 552–582. https://doi.org/10.1016/j.icarus.2013.06.006

Strobel, D. F. (2008). Titan's hydrodynamically escaping atmosphere. *Icarus*, *193*(2), 588–594. https://doi.org/10.1016/j.icarus.2007.08.014

Strobel, D. F. (2012). Hydrogen and methane in Titan's atmosphere: Chemistry, diffusion, escape, and the Hunten limiting flux principle (This article is part of a Special Issue that honours the work of Dr. Donald M. Hunten FRSC who passed away in December 2010 after a very illustrious career). *Canadian Journal of Physics*, *90*(8), 795–805. https://doi.org/10.1139/p11-131

Tokano, T., & Neubauer, F. M. (2002). Tidal winds on Titan caused by Saturn. *Icarus*, *158*, 499–515. https://doi.org/10.1006/icar.2002.6883

Vadas, S. L., & Fritts, D. C. (2005). Thermospheric responses to gravity waves: Influences of increasing viscosity and thermal diffusivity. *Journal of Geophysical Research*, *110*, D15103. https://doi.org/10.1029/2004JD005574

Waite, J. H., Niemann, H., Yelle, R. V., Kasprzak, W. T., Cravens, T. E., Luhmann, J. G., et al. (2005). Ion neutral mass spectrometer results from the first flyby of Titan. *Science*, *308*, 982–986. https://doi.org/10.1126/science.1110652

Westlake, J. H., Bell, J. M., Waite, J. H., Johnson, R. E., Luhmann, J. G., Mandt, K. E., et al. (2011). Titan's thermospheric response to various plasma environments. *Journal of Geophysical Research*, *116*, A03318. https://doi.org/10.1029/2010JA016251

Yelle, R. V. (1991). Non-LTE models of Titan's upper atmosphere. *The Astrophysical Journal*, *383*, 380–400. https://doi.org/10.1086/170796